PROCEEDINGS OF SPIE

SPIEDigitalLibrary.org/conference-proceedings-of-spie

Automated detection and segmentation of follicles in 3D ultrasound for assisted reproduction

Nikhil S. Narayan, Srinivasan Sivanandan, Srinivas Kudavelly, Kedar A. Patwardhan, G. A. Ramaraju

Nikhil S. Narayan, Srinivasan Sivanandan, Srinivas Kudavelly, Kedar A. Patwardhan, G. A. Ramaraju, "Automated detection and segmentation of follicles in 3D ultrasound for assisted reproduction," Proc. SPIE 10575, Medical Imaging 2018: Computer-Aided Diagnosis, 105751W (27 February 2018); doi: 10.1117/12.2293121

SPIE.

Event: SPIE Medical Imaging, 2018, Houston, Texas, United States

Automated Detection and Segmentation of Follicles in 3D Ultrasound for Assisted Reproduction

Nikhil S. Narayan*[1], Srinivasan Sivanandan[1], Srinivas Kudavelly[1], Kedar A. Patwardhan[1] and Ramaraju GA, MD[2]
[1]Samsung R&D Institute India, Bangalore
[2]Krishna IVF Clinic, Visakhapatnam, India

ABSTRACT

Follicle quantification refers to the computation of the number and size of follicles in 3D ultrasound volumes of the ovary. This is one of the key factors in determining hormonal dosage during female infertility treatments. In this paper, we propose an automated algorithm to detect and segment follicles in 3D ultrasound volumes of the ovary for quantification. In a first of its kind attempt, we employ noise-robust phase symmetry feature maps as likelihood function to perform mean-shift based follicle center detection. Max-flow algorithm is used for segmentation and gray weighted distance transform is employed for post-processing the results. We have obtained state-of-the-art results with a true positive detection rate of >90% on 26 3D volumes with 323 follicles.

Keywords: Assisted Reproduction, Transvaginal Ultrasound, IVF, Follicle Quantification

1. INTRODUCTION

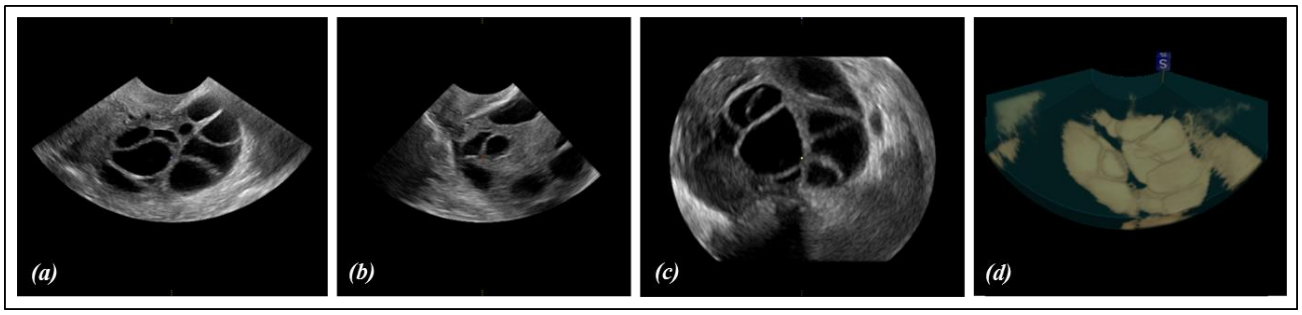

Figure 1. (a-c) Multi-planar views of 3D TV-US image of the ovary; and (d) 3D rendering of the follicles in inversion mode.

In the female reproductive system, follicles are the sites of synthesis of the oocyte and are present in the ovary. The quality of oocyte is directly proportional to the size of the follicle at the time of ovulation. Higher the quality of oocytes, better are the prospects of a successful pregnancy. About 9-12 follicles are synthesized in the ovary in a single menstrual cycle. Only one grows enough to house the oocyte that is released in the middle of the monthly cycle. Arrested growth of the follicles indicates abnormalities such as the Poly Cystic Ovarian Syndrome [1].

In female infertility, where the follicles cease to grow, In-Vitro Fertilization (IVF) is one of the options for infertility treatment. In IVF treatment, the follicles are stimulated by external administration of hormones. The goal of IVF is to have as many follicles to grow as large as possible. As a rule of thumb, all the follicles that attain a size greater than 15mm are aspirated at the end of the IVF cycle. A typical IVF cycle lasts anywhere from 11 to 16 days with the follicle growth hormones administered periodically during the cycle. One of the key factors in determining the dosage of hormones is the count and the size of the follicles. The sizes of follicles are quantified using the following parameters: diameter of the relaxed sphere (dV), length of major axis, length of minor axis, average length and follicle volume [2].

The modality of choice for follicle quantification is 3D Transvaginal Ultrasonography (3D TV-US). Figure 1 shows three cut planes (called the multi-planar views) of a 3D TV-US volume of the ovary and its corresponding 3D rendered image. It can be observed from the figure that follicles appear as hypo-echoic structures with a thin layer of hyper echoic ovarian stroma separating each follicle. The ovarian boundary itself appears as a hyper-echo around the follicles.

Medical Imaging 2018: Computer-Aided Diagnosis, edited by Nicholas Petrick, Kensaku Mori, Proc. of SPIE Vol. 10575, 105751W · © 2018 SPIE · CCC code: 1605-7422/18/$18 · doi: 10.1117/12.2293121

Traditionally, follicle quantification is done manually, where the examining sonographer identifies the plane in 3D volume where the follicle visually has the maximum diameter and measures its size with the help of calipers on the ultrasound machine. Manual quantification of follicle size and count is subject to large inter-observer variations and is time consuming [3]. There have been attempts in the past to automate the process and solve the problems associated with the manual quantification of follicles. The algorithms proposed in literature [4,5], for automated follicle quantification are: (a) sensitive to noise; (b) dependent on the image acquisition settings; (c) limited by low detection rates (50% in [4] and 80% in [5]); and (d) dependent on proper region of interest (ROI) selection. We propose a novel algorithm to detect and segment follicles that addresses the limitations of the existing approaches for accurate follicle quantification.

2. METHODS

A three stage pipeline comprising of detection, segmentation and a post-processing is employed to quantify the follicles as shown in Figure 2.

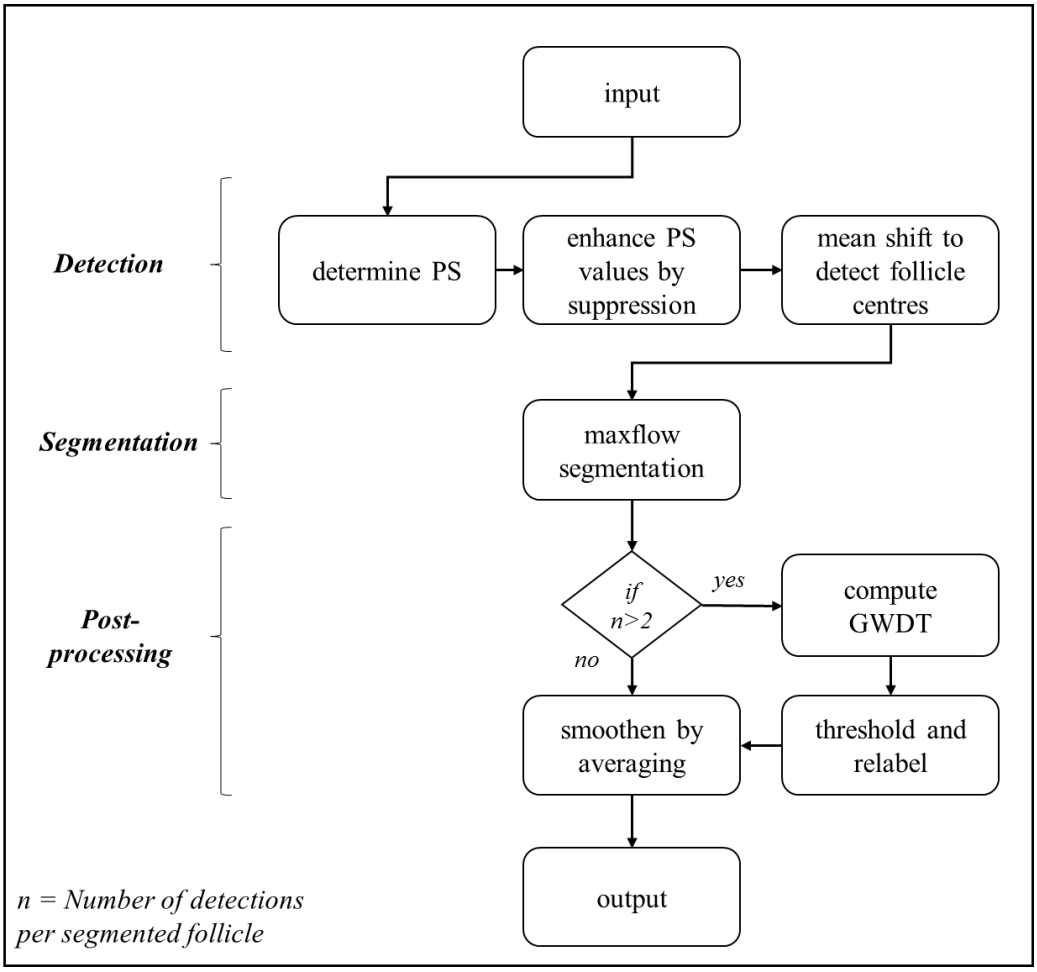

Figure 2. Flow Diagram of the algorithm.

2.1 Detection

In order to obtain accurate quantifications, the follicle detection has to be robust to speckle noise and imaging artefacts. The ovarian stroma in between the follicles appears to be diffuse in the presence of shadow artefacts. In order to detect follicles in the presence of noise and diffuse boundaries, we employ features derived from local phase. Local phase provides information regarding the state of the signal at any given instant in time and is invariant to signal energy. The use of local phase to perform tissue characterization based on echogenicity has been successfully demonstrated in [6,7].

The Phase Symmetry (PS) map derived from local phase is a useful feature to detect salient hypo-echoic enclosed structures in ultrasound images [8].

The PS at a voxel is defined as:

$$PS = \frac{\sum_s \lfloor [|e_s| - |o_s|] - T \rfloor}{\sum_s \sqrt{(e_s^2 + o_s^2) + \epsilon}} \tag{1}$$

$$o_s = \sqrt{(e_s * h_1)^2 + (e_s * h_2)^2 + (e_s * h_3)^2} \tag{2}$$

where, s is the scale factor, T is the noise tolerance constant, e_s is the 3D ultrasound image bandpass filtered with a log Gabor filter and o_s is obtained as in Eq.(2). Here, h_1, h_2 and h_3 are the antisymmetric filters used to obtain the Riesz transform of the bandlimited signal e_s [9].

A distinct PS peak is not observed inside the follicles due the homogeneity in echogenicity of the follicles. To obtain a distinct peak, the PS map is enhanced by binary thresholding and smoothening. Figure 3 shows the PS map before and after enhancement. It can be seen from the figure that, enhancing the PS map also suppresses the contributions from the non-follicular region to the detection process. This ensures that the number of false positive detections remains low at the end of the detection stage.

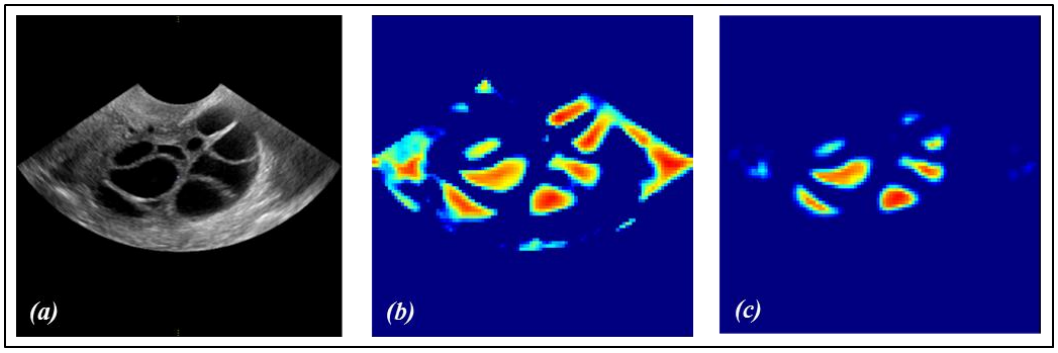

Figure 3. Enhancing PS map. (a) Input image; (b) PS map; and (c) PS map after enhancement.

Having obtained the PS maps, the follicle centers are detected by employing a modified version of the mean-shift algorithm of [10]. Here, the PS map is used as the likelihood function instead of voxel intensities in the mean shift update equation given by Eq. (3).

$$x_{k+1} = \frac{\sum_{i \in N(x_k)} x_k PS_i}{\sum_{i \in N(x_k)} PS_i} \tag{3}$$

where, PS_i is the PS value at i in the neighborhood N of the data point x under consideration. Mean shift algorithm helps in: (a) determining multiple detections of same follicle; (b) splitting merged follicles in the post processing stage of the algorithm. Random seed points are initialized in the 3D ultrasound image and the mean shift update of Eq. (3) is enforced on all the points until convergence ($x_{k+1} = x_k$). The points of convergence are chosen as follicle centers for segmentation initialization. Figure 4 illustrates the follicle detection process using modified mean shift.

2.2. Segmentation

Post detection of follicle centers, the segmentation is obtained by applying a max-flow algorithm [11]. The follicle center detections are given as initialization seed points for the segmentation algorithm. The flow graph is constructed by connecting the detected follicle center voxels to flow source and a bounding box around the detection to flow sink. Each of the voxels within the bounding box is connected to the graph via a 26 voxel neighborhood. The edge weight between neighboring voxels a, b is assigned as in Eq. (4) where I_a and I_b are the intensity values of the corresponding voxels and σ is a constant.

$$edgeweight(a,b) = e^{\frac{-(I_a - I_b)^2}{2\sigma^2}} \quad (4)$$

Figure 5b shows the results of applying max-flow segmentation algorithm using the follicle centers as initialization points. The segmented output is labeled by connected components as shown in Figure 5c.

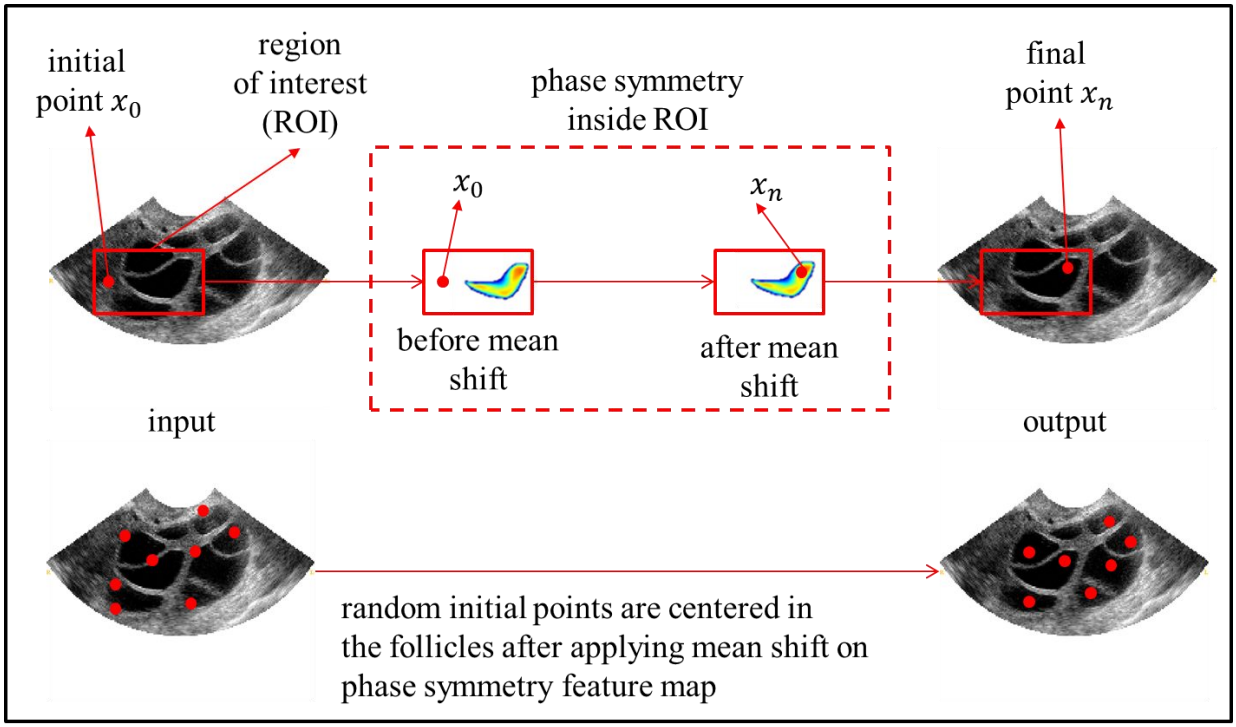

Figure 4. Illustration of mean shift based follicle detection.

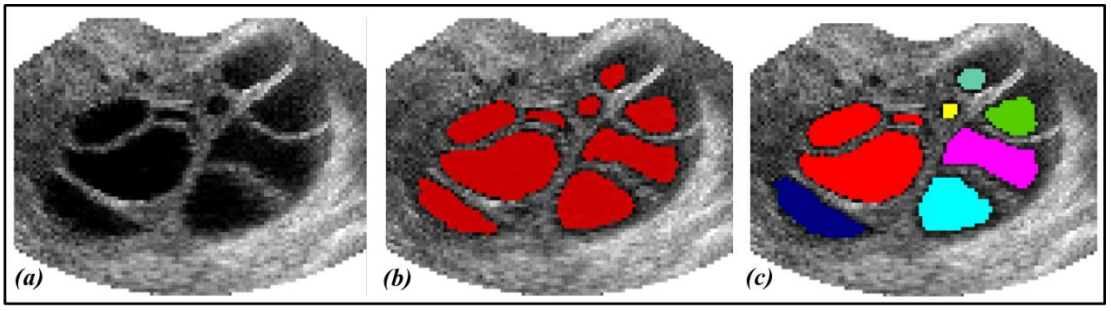

Figure 5. (a) Input image; (b) max-flow segmentation output; (c) segmentation labelled by connected components.

2.3 Post-processing

It can be seen from Figure 6a, that the segmentation algorithm merges some follicles that have diffuse boundaries. The follicles merged by segmentation are detected by checking for the presence of multiple follicle centers (obtained from the detection stage) within a single segmentation label. In order to split the merged follicles, Gray Weighted Distance Transform [12] is computed using a binary mask of merged follicles and a statistical threshold is applied to split the merged follicles as shown in Figure 6b and 6c. Figure 6d shows the results after splitting the follicles merged in Figure 6a. The surface mesh of the segmented follicles is extracted for quantification and visualization. Figure 7 shows the segmentation results with 3D mesh rendering of the follicles.

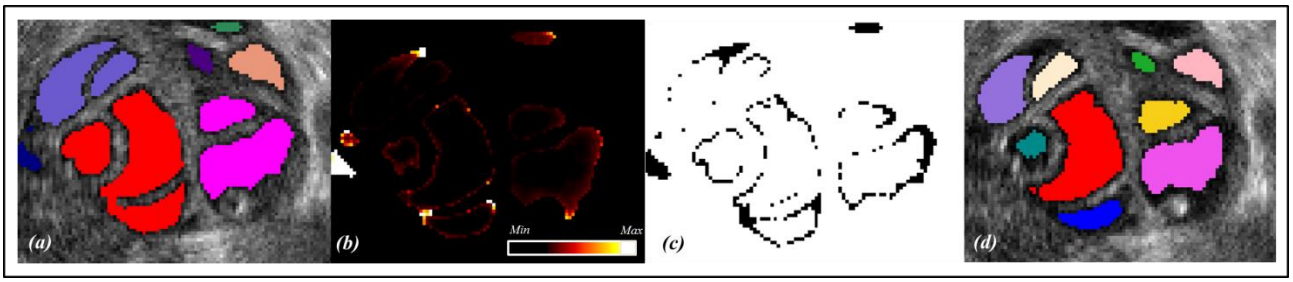

Figure 6. (a) Segmentation with merged follicles (in red); (b) GWDT image; (c) GWDT mask obtained after applying statistical threshold; (d) Merged follicles split and relabeled after post-processing.

3. RESULTS AND DISCUSSION

Experiments were conducted on a dataset comprising of 26 3D TV-US volumes. The datasets were obtained with consent from Krishna IVF clinic, Vishakhapatnam, India in accordance with the guidelines established by the Institutional Review Board at Krishna IVF. The algorithm was implemented in C++ on an Intel Core i7 processor with 8GB RAM.

Manual segmentations obtained from experts are considered as ground truth (GT) to evaluate the performance of our algorithm. The manual segmentations were collected using ITK-SNAP [13]. Detection is considered to be True Positive (*TP*) if there is an overlap with the GT. Detection with no overlap with GT is considered to be False Positive *(FP)* and GT follicles that are not detected are considered to be False Negative *(FN)*. We have obtained a detection true positive rate ($TP/(TP+FN)$) of >90% for 323 follicles greater than 4mm in diameter (Table 1). Table 2 shows the comparison of our algorithm with existing state of the art methods.

The segmentation accuracy is determined by the Dice coefficient (DSC) given by $(\mathcal{S} \cap \mathcal{G})/(\mathcal{S} \cup \mathcal{G})$ where $\mathcal{S}$ is the set of all pixels belonging to the segmented follicle and $\mathcal{G}$ is the set of all pixels belonging to the GT follicle.

Table 1: Performance evaluation results

	Detection Rates in #Follicles	
Follicle Diameter	*4mm-12mm*	*>12mm*
GT	240	83
True Detections	212	80
% Detection	90.4	96.4
% DSC	70.0	78.6

Table 2: Comparison with state-of-the-art*

Algorithm	**Detection Rate**
Jörgner et al., [4]	51.9 %
Chen T et al., [5]	80.3 %
Our approach	90.4 %

* The results are as reported in the respective literature.

4. CONCLUSION AND FUTURE WORK

We have presented a novel algorithm that can perform follicle quantification by efficiently tracking follicle centers for detection and segmentation. Further, the clinical significance of the algorithm is demonstrated in our longitudinal studies of follicular growth [14]. Detecting the antral follicles (<4mm) and improving the segmentation accuracy are some of the next steps of this research work.

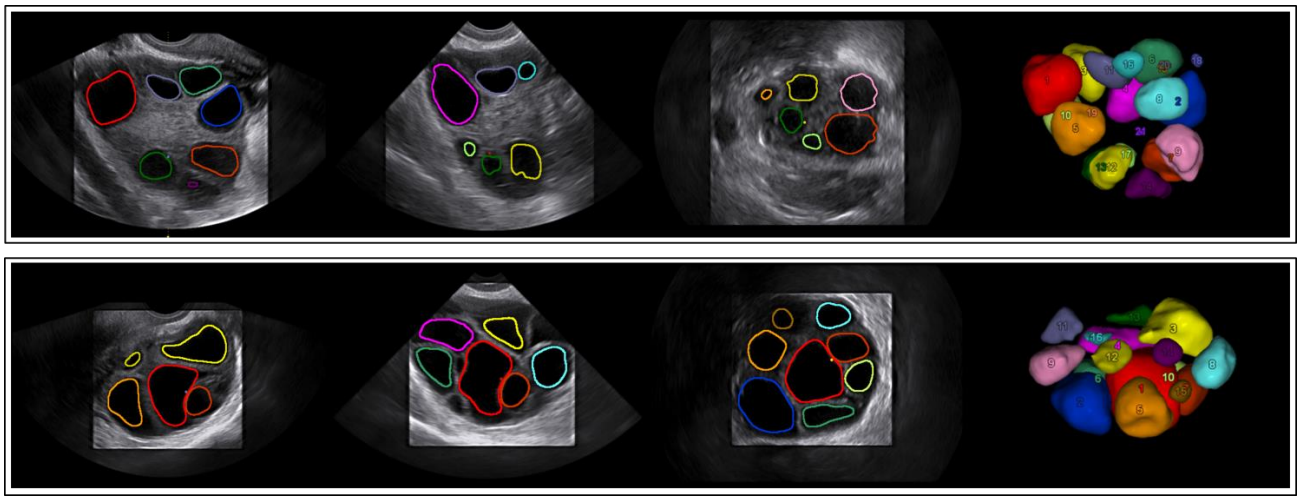

Figure 7. Detection & Segmentation results with 3D rendering of follicles.

REFERENCES

1. Fr, D. Dewailly, and R. Tarlatzis. "Revised 2003 consensus on diagnostic criteria and long-term health risks related to polycystic ovary syndrome." Fertility and sterility 81, no. 1 (2004).
2. Stadtmauer, Laurel A., and Ilan Tur-Kaspa. "Ultrasound imaging in reproductive medicine." Springer-Verlag London Limited, (2014).
3. Vandekerckhove, Frank, Victoria Bracke, and Petra De Sutter. "The value of automated follicle volume measurements in IVF/ICSI." Frontiers in surgery 1 (2014).
4. Jörger I, Scherleitner E. "SonoAVC Studies on automated detection and measurements of hyper-stimulated follicles utilizing a new algorithm." GE Medical Systems Ultrasound & Primary Care Diagnostics (2008).
5. Chen, Terrence, Wei Zhang, Sara Good, Kevin S. Zhou, and Dorin Comaniciu. "Automatic ovarian follicle quantification from 3d ultrasound data using global/local context with database guided segmentation." In Computer Vision, 2009 IEEE 12th International Conference on, pp. 795-802. IEEE, (2009).
6. Narayan, Nikhil S., Pina Marziliano, Jeevendra Kanagalingam, and Christopher GL Hobbs. "Speckle Patch Similarity for Echogenicity-Based Multiorgan Segmentation in Ultrasound Images of the Thyroid Gland." IEEE journal of biomedical and health informatics 21, no. 1 (2017): 172-183.
7. Rahmatullah, Bahbibi, Aris T. Papageorghiou, and J. Alison Noble. "Integration of local and global features for anatomical object detection in ultrasound." In International Conference on Medical Image Computing and Computer-Assisted Intervention, pp. 402-409. Springer, Berlin, Heidelberg, 2012.
8. Patwardhan, Kedar A. "Symmetry and appearance based automated detection of salient anatomical regions in ultrasound." In Engineering in Medicine and Biology Society (EMBC), 2012 Annual International Conference of the IEEE, pp. 4426-4428. IEEE, 2012.
9. Kovesi, Peter. "Symmetry and asymmetry from local phase." In Tenth Australian joint conference on artificial intelligence, vol. 190, pp. 2-4. Citeseer, 1997.
10. Fukunaga, Keinosuke, and Larry Hostetler. "The estimation of the gradient of a density function, with applications in pattern recognition." IEEE Transactions on information theory 21, no. 1 (1975): 32-40.
11. Boykov, Yuri, and Vladimir Kolmogorov. "An experimental comparison of min-cut/max-flow algorithms for energy minimization in vision." IEEE transactions on pattern analysis and machine intelligence 26, no. 9 (2004):1124-1137.
12. Soille, Pierre. "Generalized geodesy via geodesic time." Pattern Recognition Letters 15, no. 12 (1994): 1235-1240.
13. Yushkevich, Paul A., Joseph Piven, Heather Cody Hazlett, Rachel Gimpel Smith, Sean Ho, James C. Gee, and Guido Gerig. "User-guided 3D active contour segmentation of anatomical structures: significantly improved efficiency and reliability." Neuroimage 31, no. 3 (2006): 1116-1128.
14. Subbarao, N., R. GA, K. A. Patwardhan, and S. R. Kudavelly. "EP27. 03: Longitudinal volumetric analysis of follicular growth." Ultrasound in Obstetrics & Gynecology 50, no. S1 (2017): 384-384.